ULUSLARARASI 3B YAZICI TEKNOLOJİLERİ
VE DİJİTAL ENDÜSTRİ DERGİSİ
INTERNATIONAL JOURNAL OF 3D PRINTING
TECHNOLOGIES AND DIGITAL INDUSTRY

ISSN:2602-3350 (Online)
URL: https://dergipark.org.tr/ij3dptdi

MONITORING PEI PRODUCTION PARAMETERS ON A CUSTOM-MADE 3D PRINTER: AN INSIGHT INTO PHYSICAL AND MECHANICAL PROPERTIES

Yazarlar (Authors): Alptekin Yıldız

Bu makaleye şu şekilde atıfta bulunabilirsiniz (To cite to this article): *Yıldız A., "Monitoring PEI Production Parameters On A Custom-Made 3D Printer: An Insight Into Physical And Mechanical Properties" Int. J. of 3D Printing Tech. Dig. Ind., 8(2): 287-302, (2024).*

DOI: 10.46519/ij3dptdi.1493819

Araştırma Makale/ Research Article

Erişim Linki: (To link to this article): https://dergipark.org.tr/en/pub/ij3dptdi/archive

MONITORING PEI PRODUCTION PARAMETERS ON A CUSTOM-MADE 3D PRINTER: AN INSIGHT INTO PHYSICAL AND MECHANICAL PROPERTIES

Alptekin Yıldız[a,b]*

[a] Istanbul Technical University, Aviation Institute, Türkiye
[b] Istanbul Technical University, Aerospace Research Center, Türkiye

* *Corresponding Author: alptekin.yildiz@itu.edu.tr*

(**Received:** 01.06.2024; **Revised:** 12.08.2024; **Accepted:** 15.08.2024)

ABSTRACT

This study investigates the impact of production parameters on the quality of 3D-printed polyetherimide (PEI) samples using a custom-made 3D printer. In contrast to traditional optimization approaches, this research emphasizes the variability of outcomes despite maintaining fixed parameters such as nozzle and bed temperatures and slicer options. The study involves real-time monitoring of factors including nozzle, bed, and chamber temperatures, as well as relative humidity during the production process. Each layer was photographed individually to analyze its impact on the final product. Detailed physical and mechanical analyses revealed significant deviations in dimensions and flexural modulus, with a 10% loss in density and nearly 25% loss in flexural modulus in lower-performing samples compared to the best results. Results show correlations between critical parameters and product quality, underscoring the necessity for proper preparation and precise control. Furthermore, the research proposes a new method to geometrically represent the manufacturing process in a time-independent way using collected sensor data in 3D printing. This approach provides valuable insights for future studies aimed at optimizing additive manufacturing processes and enhancing the application of high-performance thermoplastics in high-tech fields such as aerospace and defense industries.

Keywords: Additive Manufacturing, Material Extrusion, Fused Filament Fabrication, Polyetherimide, DMA.

1. INTRODUCTION

Additive manufacturing (AM) has revolutionized industrial production processes in recent years, providing flexibility and cost savings in both the design and production stages. The advantages of AM technologies are not only evident in prototyping but also extend to final product manufacturing. In particular, AM methods enable the rapid and precise production of parts with complex geometries, thereby making production processes more adaptable and economical [1-3]. Among the various AM technologies, Fused Filament Fabrication (FFF), classified under Material Extrusion (MEX), has struggled to gain traction in high-tech sectors due to disadvantages such as limited material diversity and lower mechanical strengths compared to traditional manufacturing techniques. However, recent advancements have begun to address these challenges. The advent of high-performance thermoplastics like polyetherimide (PEI) and polyether ether ketone (PEEK), along with composites enhanced with various nano- and micro-additives, has paved the way for the application of FFF technology in high-tech areas, including aerospace and defense industries. These materials offer superior thermal stability, mechanical strength, chemical resistance, and multifunctional properties, making them suitable for demanding applications [4-6]. In sectors with stringent requirements, maintaining consistent quality control and physical and mechanical properties throughout the additive manufacturing process is crucial [7-8]. Consequently, monitoring and controlling relevant parameters during the production of high-performance thermoplastics has become vital for both production efficiency and product reliability.

In FFF, extensive analytical, numerical, and experimental studies have examined the fundamental production parameters, general characteristics, and limitations of all production stages [9-12]. Additionally, optimization studies employing parametric and statistical approaches for various additive manufacturing technologies are well-documented in the literature [13,14]. On the other hand, research focused on high-performance materials such as PEI and PEEK has consistently demonstrated their superior thermal stability and mechanical strength, particularly under optimal printing conditions [15]. The influence of nozzle temperature and structural orientation on the performance of PEEK and PEI is well-documented, showing significant improvements in mechanical properties when these parameters are carefully controlled [16]. Additionally, it has been shown that optimal infill parameters play a minimal role in the mechanical performance of PEI parts, which is particularly beneficial for weight-sensitive applications in the aerospace industry [17]. Furthermore, detailed investigations into process parameters that enhance print quality by optimizing the thermal and mechanical properties of PEEK and PEI blends have provided valuable insights into the production of high-quality components using FFF [18-20]. These studies underscore the critical role of temperature control, structural orientation, and material blends in achieving superior part quality in additive manufacturing.

Several studies have emphasized the importance of monitoring and controlling key parameters that influence the quality and physical properties of the final product. For instance, Vanaei et al. [21] highlighted the critical role of temperature control in optimizing the crystallinity and mechanical integrity of 3D prints produced via the FFF process. Their research demonstrated that monitoring filament temperature profiles is essential for enhancing interlayer adhesion and overall print quality. Similarly, Sgrulletti et al. [22] investigated the effects of bed temperature on the microstructure and tensile properties of FFF prints made from polyamide 6, utilizing thermal and optical live monitoring techniques. Their findings revealed that precise control of bed temperature significantly improves mechanical properties and morphology, with the use of integrated live monitoring systems resulting in a 70% increase in Young's modulus and a 79% improvement in tensile strength. Alatefi et al. [23] assessed the benefits of multivariate statistical quality monitoring in additive manufacturing. Their research demonstrated that the MEWMA (Multivariate Exponentially Weighted Moving Average) control chart reduces production defects, thereby improving the quality and stability of the FFF process. A transformation algorithm was employed to normalize data distribution, and MEWMA parameters were optimized using a novel heuristic technique, proving effective in maintaining process stability. Özsoy and Aksoy [24] investigated the effectiveness of artificial intelligence and image processing techniques in FFF printing. Their study showed that these techniques substantially enhanced the accuracy and quality control of the printing process, achieving a prediction accuracy of 92.5% for process parameters. By employing AI algorithms and image processing techniques, defects were swiftly identified, thereby increasing process efficiency.

Researchers investigating the critical effects of production parameters on the final product naturally aim to identify the optimal settings. The general assumption is that end users will apply these optimal parameters to achieve the best possible results. However, the production mechanism in AM is highly complex, influenced by multiple factors, many of which are non-linear. Parameters that are expected to remain constant may vary for various reasons, leading to deviations from the expected outcomes. As highlighted in the literature, real-time monitoring during production enhances the understanding and control of these complex processes. Therefore, further research is essential to optimize quality in the additive manufacturing of high-performance thermoplastics such as PEI. This includes developing systematic approaches for monitoring and controlling these parameters throughout the production process to ensure consistent and high-quality outputs.

This study intends to contribute to both academic literature and industrial practices by critically examining the FFF production process for high-performance thermoplastics, specifically PEI, under controlled yet naturally fluctuating environmental conditions. Unlike previous research that focuses primarily on

optimizing fixed production parameters, this work addresses the complexities that arise from variable chamber conditions, such as temperature and relative humidity, which inherently impact the production process. By systematically tracking and analyzing these parameters throughout the 3D printing process, this study provides a novel perspective on how real-time environmental monitoring influences the physical and mechanical properties of the final product. The adoption of ASTM D790 standard sample geometry, combined with advanced data collection techniques, enhances the robustness and applicability of this approach. This study not only deepens the understanding of FFF technology in the context of high-performance materials but also lays the foundation for future research aimed at improving the reliability and quality control of additive manufacturing processes in highly demanding sectors such as aerospace and defense.

2. MATERIAL AND METHODS

2.1. Filament Production

The polyetherimide (PEI - ULTEM™ RESIN 1010) granules was sourced from Sabic. The chemical formula of PEI is $C_{37}H_{24}O_6N_2$, with a density of 1.27 g/cm³ and a molecular weight of 592 g/mol. The glass transition temperature (T_g) of this material is 217 °C.

The PEI granules were subjected to a drying process in an oven at a temperature of 150 °C for a duration of eight hours. This was done to remove any residual moisture present, thereby preventing any undesirable conditions from occurring during the extrusion process. A lab-scale co-rotating twin-screw extruder was utilized to fabricate neat PEI filaments with a diameter of 1.75 mm. The extruder, manufactured by Kökbir Import & Export, features a screw diameter of 12 mm and a length-to-diameter (L/D) ratio of 22 [5]. The temperature gradient from the feed to the nozzle was meticulously controlled within the range of 310–360 °C, with a maintained screw speed of 210 rpm.

2.2. Custom-Made 3D Printer

The 3D printer (ARC-Beta) developed at the ITU Aerospace Research Center was designed to handle high-performance thermoplastics and includes several advanced features. Controlled by Marlin firmware on RAMPS 1.4, the printer employs a direct drive extruder, DyzEND-X & DyzeXtruder GT 1.75 mm kit with high-temperature sensors, compatible with a range of thermoplastic filaments, including PLA, ABS, nylon, PEEK, and PEI. Its Core-XY motion system enables precise extruder positioning. The printer is constructed with all-metal components and 3D-printed PEI parts, allowing it to reach print nozzle temperatures of up to 500 °C and bed temperatures of up to 200 °C. The device offers a print area of 25 × 25 cm and a print volume of 25 × 25 × 30 cm, housed within an 80 × 80 × 80 cm enclosed chamber. The chamber can reach temperatures up to 85K °C while maintaining a relative humidity of 10% or lower. Furthermore, the printer is equipped with remote control capabilities via OctoPrint software and integrated cabin temperature and humidity measurement. The design of the 3D printer can be seen in Figure 1.

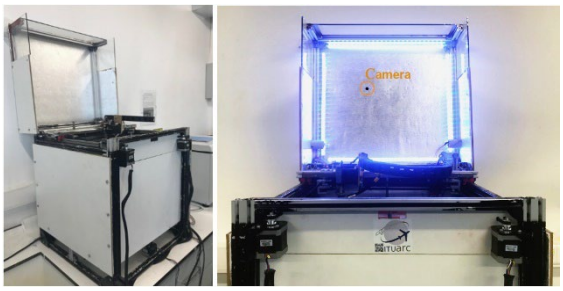

Figure 1. The custom-made 3D Printer ready for high-performance thermoplastics.

To understand the effects of production parameters on the printed product, the objective was to collect visual and real-time signal data during printing. Consequently, additional features were incorporated into the 3D printer cabinet. One key enhancement is a camera mounted above the printing bed, allowing it to capture images of each entire layer during printing. The Raspberry Pi Camera Module V2 was selected for this purpose and integrated with the 3D printer using a Raspberry Pi 3 control board, which enables remote control of the printer and the incorporation of mechanisms to capture images. To ensure optimal layer imaging, LED strips were installed for in-cabinet lighting. Another feature added to the 3D printer is the BME280 sensor. This sensor complements the monitoring of bed and nozzle temperatures by measuring the instantaneous chamber temperature and humidity, considering the bed temperature and cabinet insulation. This setup allows for the simultaneous capture of each layer's image and real-time recording of

nozzle, bed, and chamber temperatures, as well as chamber humidity, throughout the printing process.

2.3. 3D Printed Sample Production

For the test specimens printed using a 3D printer, the ASTM D790 standard was adopted. Specimens measuring 65 × 13 × 3 mm were produced in accordance with this standard, which is designed to determine dynamic mechanical properties (Dynamic Mechanical Analysis - DMA) by the three-point bending method for plastics. Based on experience [25], the optimal parameters for printing the test specimens are as follows:

- Nozzle diameter: 0.4 mm
- Nozzle temperature: 375°C
- Bed temperature: 160°C.
- Layer height: 0.2 mm
- Number of layers: 15
- Number of perimeter lines: 3
- Infill: 100% with a ±45° rectangle pattern
- Outline overlap:15%
- Skirt (First layer): 10 outlines without offset
- Speed: 30 mm/ s, %50 reduced for 1st layer

Figure 2 illustrates the sample dimensions and the specimen prepared for 3D printing using the slicing program.

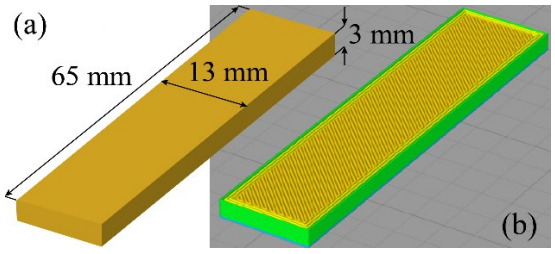

Figure 2. (a) Dimensions and (b) layered (sliced) view of a DMA specimen conforming to ASTM D790 Standard prepared for 3D printing using the Simplify3D slicing program.

Each printing process followed a specific protocol. First, the glass surface on the bed was thoroughly cleaned with alcohol. The bed was then carefully aligned to be exactly perpendicular to the nozzle plane (or parallel to the ground). The distance between the nozzle and the bed was checked at a minimum of three points using a feeler gauge for the z-end point to ensure precise positioning. A very thin layer of Nano Polymer Adhesive from Vision Miner was applied to the surface using a brush. Both the nozzle and the bed were preheated, and after a designated waiting period, the print-specific protocol (gcode) prepared with Simplify3D software was initiated. During printing, at the end of each layer, the extruder was moved to the side using a command added to the gcode, and photographs with a resolution of 3280 × 2464 were taken using the camera module, capturing the entire sample. Upon completion of the printing process, the bed and chamber were allowed to cool, and the sample was carefully removed. The production steps described were then repeated for the next print.

2.4. Characterization

Geometric measurements of the samples included width, thickness, and length. Using precision calipers, measurements were taken at three different points: the center and near both edges of the relevant surfaces (Figure 3). These values were then averaged with standard deviations to obtain the final dimensions.

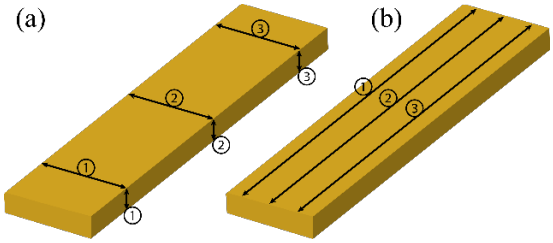

Figure 3. Measurement points for (a) width, thickness and (b) length on each specimen.

The mass of the samples was measured using an analytical balance. Density calculations were then performed using the mass data and the averages of the dimensions of the relevant sample.

Flexural modulus measurements were performed using a TA Instruments DMA 850 (New Castle, DE) following the ASTM D790 standard. The test utilized a 3-point bending fixture with a span of 50 mm. The measurement parameters included a crosshead speed of 0.05 mm/min and an initial force of 0.1 N.

2.5. Collecting Sensor Data from 3D Printer

In the study, in addition to the photographs taken during the production of each layer, a data processing algorithm was developed in Python to collect and organize data by processing log files generated by the OctoPrint and Marlin Control software. The algorithm, written in Python, reads data from two different log files

(octoprint.log and serial.log), parses the information, and structures it into a pandas DataFrame. The resulting data is then made available for analysis.

The contents of the log files are as follows:
Octoprint.log:
- This log file, generated by OctaPrint software, contains information about the printer's state changes (e.g., 'Starting', 'Printing'), events and enclosure temperature and humidity readings from the BME280 sensor.
- Each line includes a timestamp, the type and detailed information about the event.

Example Lines:
2024-01-10 07:58:17,267 –
octoprint.util.comm - INFO - Changing monitoring state from 'Starting' to 'Printing'
2024-01-10 07:58:17,276 –
octoprint.filemanager.analysis - DEBUG - Pausing analysis
2024-01-10 08:10:15,387 –
octoprint.plugins.enclosure - DEBUG - BME280 result: 79.2 | 4.6

Serial.log:
- This log file, generated by Marlin firmware, contains serial communication commands and feedback between the printer and the software.
- It includes sent and received commands, temperature readings, layer and coordinate information, and sensor data (e.g., nozzle and bed temperature).

Example Lines:
2024-01-10 07:58:17,257 –
Changing monitoring state from 'Starting' to 'Printing'

2024-01-10 07:58:17,309 –
Send: N1 G90*17
2024-01-10 07:58:17,377 –
Recv: ok T:375.1 /375.0 B:160.0 /160.0 @:87 B@:55
2024-01-10 07:58:19,285 –
Recv: X:0.00 Y:220.00 Z:0.00 E:3663.27 Count A: 17600 B:-17600 Z:0

The algorithm designed to systematically retrieve data from these two documents works through the following steps:

1. The log files are read line by line using the command ‘with open(filepath, 'rt') as in_file:’ and each line is appended to a list. This process is performed separately for both `octoprint.log` and `serial.log` files.

2. Regular expressions (regex) are used to extract the necessary data from each line. For example, timestamps are parsed using the ‘pd.to_datetime()’ function. The ‘re.compile()’ and ‘re.search()’ functions are used to find lines that match specific patterns.

3. Sensor data in "serial.log" and "Octoprint.log" are extracted from specific command and feedback lines in two separate locations.

4. The timestamps are converted to seconds and normalized, enabling the seamless integration of data from different sensors for comprehensive analysis.

5. The parsed data is converted into a pandas DataFrame and then exported as a csv file.

As a result, X-Y position of extruder, nozzle, bed and chamber temperatures, and relative humidity data were collected for 10 different samples, with 3,375 data points each.

2.6. Data Analysis Methodology
Python was employed extensively for data preparation, visualization, and statistical analyses, including correlation and ANOVA in this study. The data processing workflow utilized a combination of Python libraries to ensure thorough and accurate analysis. The pandas library was used for data manipulation, cleaning, and structuring, while numpy facilitated numerical operations and data array management. The scipy library provided tools for statistical computations, including correlation and ANOVA, whereas the statsmodels library was used for advanced statistical modeling and hypothesis testing. For visualization, matplotlib and seaborn libraries were used for initial data visualization and exploratory analysis, although these figures are not included in the article to save space. All final graphs presented in this article were generated using Origin Pro to ensure publication-quality figures.

3. RESULTS AND DISCUSSION

3.1. Dimensional Analysis of 3D-Printed Samples

The results of the geometric measurements of PEI samples produced with the 3D printer using the same parameters can be seen in the Figure 4 with deviation values.

The average dimensions of the 65×13×3 mm samples were 64.51 ± 0.10 mm for length, 12.87 ± 0.09 mm for width, and 2.91 ± 0.04 mm for thickness. Although the differences are at the micron level, the targeted dimensions were not fully achieved, resulting in slightly smaller product sizes than expected. On the other hand, considering the density value of 1.27 g/cm³ for PEI, mass values of 2.68 ± 0.15 g were measured, whereas the expected mass is approximately 3.22 g (Figure 4d). The average density value, calculated based on all relevant measurements, was determined to be 1.11 ± 0.06 g/cm³ (Figure 4e).

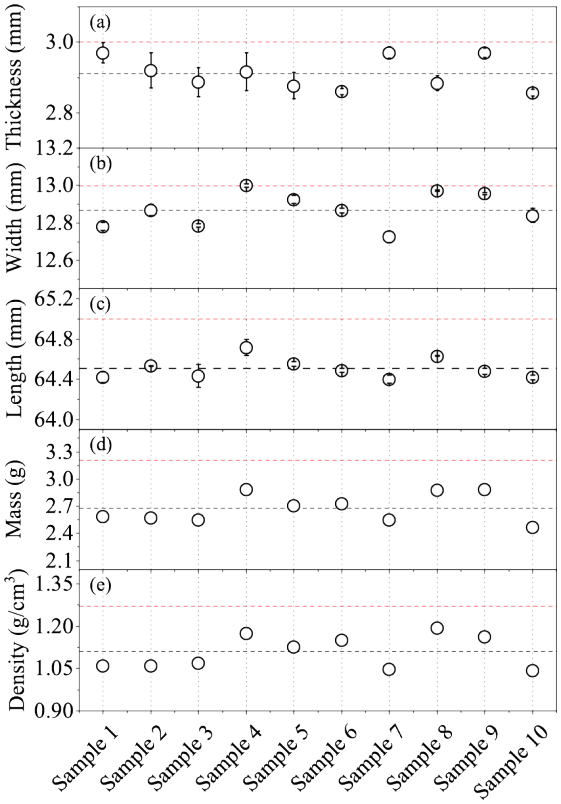

Figure 4. (a) Thickness, (b) Width, (c) Length, (d) Mass values, and (e) Density calculations of 3D-printed samples. The dimensional plots (a-c) present values with deviation lines. In all plots, the target values (red) and average values (black) of all samples are indicated by horizontal dashed lines.

The slightly lower than expected average values can be attributed to the *Extrusion Multiplier*, a production parameter that can vary for each filament type. This parameter addresses the issue where the filament is not extruded to the correct length due to various physical properties such as diameter and viscosity. For instance, if 10 mm of thermoplastic is expected to be extruded from the nozzle by feeding a certain amount of filament into the extruder, but the actual extrusion falls short, a simple multiplier value (e.g., 1.05) can be applied to push the filament further, achieving the required 10 mm. This adjustment allows the average dimensions of the produced parts, whether above or below the target, to be brought to the desired specifications. Although achieving these targeted values was confirmed in additional studies, the focus of this study is not on the absolute values themselves, but rather on examining the reasons for the deviations observed around the average values.

3.2. Flexural Moduli Results

The flexural moduli of the 3D-printed specimens were determined from the slope of the stress (σ_E) and strain (ε) curves. After applying linear curve fitting, moduli values were obtained for all specimens. It should be noted that these values are independent of the specimen geometry. In the measurements, the geometric dimensions of each specimen were entered into the TA Instrument's TRIOS software and the specimen lengths were fixed at 50 mm due to the span value of the fixture.

Table 1. The flexural moduli of 3D-Printed PEI samples.

Sample #	Flexural Modulus (MPa)
Sample 1	1808.8
Sample 2	1797.4
Sample 3	1967.1
Sample 4	2387.6
Sample 5	2381.6
Sample 6	2530.4
Sample 7	1816.2
Sample 8	2550.0
Sample 9	2328.9
Sample 10	1941.4

The flexural moduli values with an average value of 2150.93 ± 295.97 MPa are presented in Table 1 for the samples. The distribution of

relatively low, geometry-independent values clearly highlights the anisotropic and complex nature of additive manufacturing and underscores the motivation for this study.

3.3. Relationship Between Flexural Moduli and Physical Properties

Pearson, Spearman, and Kendall correlation analyses were employed to investigate the relationships between Flexural Moduli (FM) and other physical properties, including Thickness, Width, Length, Mass, and Density. Prior to the analysis, the data distribution and adherence to normal distribution were assessed through histograms and Q-Q Plots. However, these visualizations were omitted from the article to conserve space. The distribution of FM, Width, Mass, and Density variables closely approximated a normal distribution, while Thickness and Length variables exhibited some deviations. Scatter plots (Figure 5) were used to visually represent the relationships between FM and other physical characteristics, revealing negative correlations between FM and Thickness and positive correlations between FM and Width, Length, Mass, and Density.

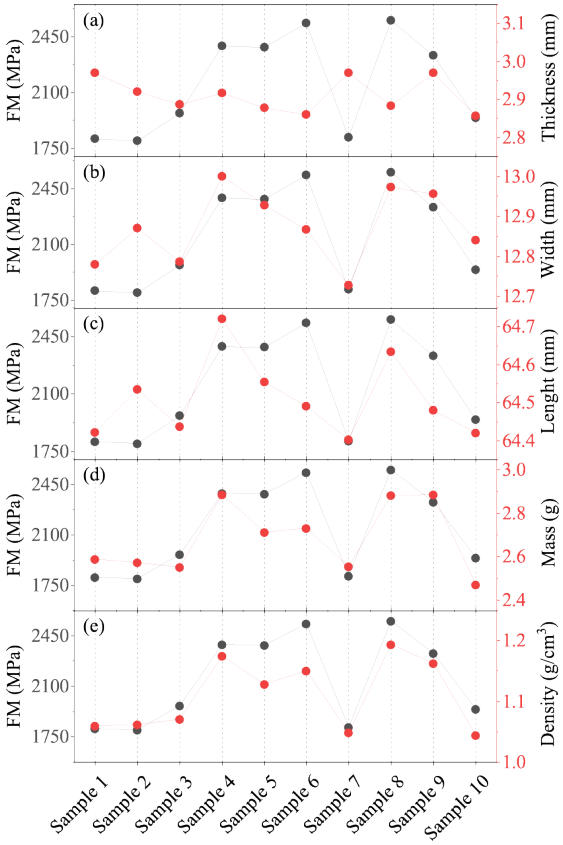

Figure 5. Flexural Moduli plots vs (a) Thickness, (b) Width, (c) Length, (d) Mass and (e) Density.

The correlation analysis results, conducted using three different methods, are presented in Table 2, with corresponding p-values in parentheses.

Table 2. Results of correlation analysis between flexural moduli (FM) and physical properties using Pearson, Spearman, and Kendall methods, with p-values in parentheses.

Variable	Pearson	Spearman	Kendall
Thickness	-0.4346 (0.2095)	-0.5079 (0.1340)	-0.3581 (0.1679)
Width	0.7853 (0.0071)	0.6991 (0.0245)	0.4944 (0.0482)
Length	0.6455 (0.0438)	0.6383 (0.0470)	0.5394 (0.0311)
Mass	0.8346 (0.0027)	0.6485 (0.0425)	0.4222 (0.1083)
Density	0.9428 (4.36e-5)	0.8268 (0.0032)	0.6293 (0.0119)

Pearson's correlation, which measures linear relationships between FM and other physical characteristics, showed a negative relationship between FM and Thickness, and positive relationships with Width, Length, Mass, and Density, with strong positive correlations for Density (0.942811) and Mass (0.834605). Spearman correlation, less sensitive to outliers of data, mirrored these results, with significant relationships for Width, Length, Mass, and Density ($p < 0.05$), but not Thickness ($p > 0.05$). Kendall correlation, robust to outliers, also showed positive relationships, with significant results for Width, Length, and Density ($p < 0.05$), but not for Thickness and Mass ($p > 0.05$). Overall, the strongest associations between FM and other physical properties were observed with Density and Mass. Given that the data were mostly normally distributed and exhibit linear relationships, Pearson analyses were more appropriate for revealing the relationships between variables. However, Spearman and Kendall correlations should also be considered, particularly for non-linear relationships or those deviating from normal distribution, such as Thickness and Length.

The observed relationships between physical properties and FM provide valuable insights into the additive manufacturing process. The positive correlation between FM and width, alongside the negative correlation between FM and thickness, suggests that specimens tend to

be relatively flattened and edge-spread. These characteristics indicate denser specimens with better interlayer adhesion when fully filled. Such findings imply that the pre-production distance between the nozzle and the bed may not have been uniformly adjusted across all samples, and/or the bed was not aligned perpendicularly (or parallel to the ground) to the nozzle plane. Additionally, the adhesive used to fix the samples to the bed might contribute to this issue. Uneven application of the adhesive with a brush after cleaning the surface with alcohol before each production can lead to adhesion problems to the bed and varying thicknesses.

These problems were particularly evident in the thickness measurements of the first five samples, where the thickness decreased toward one end, albeit by microns. The variations in thickness values shown in Figure 4 represent this observation. Furthermore, improperly set nozzle-to-bed spacing exacerbates anisotropy in printed products by causing *road distortion*, as noted by Turner et al [9]. In some cases, this can also lead to blockages, interrupting material flow and compromising print quality.

On the other hand, the relationship between FM and densities, along with the varying mass distributions, raises questions about the amount of polymer extruded. Two scenarios can lead to this situation: insufficient material being extruded or completely cutoff. The lower material output could result from a localized reduction in filament diameter used in the feed and/or fluctuations in production parameters that are expected to remain constant (such as the sensors monitored in this study), affecting the extrusion flow. Layer photographs were examined to identify these issues in the products.

3.4. Analysis of Layer Photographs

A total of 150-layer photographs, 15 from each sample, were collected at the end of production. Each layer was meticulously examined to check for proper production. Particular attention was paid to any deficiencies in layer production and the specific areas where they occurred. The FM values were considered during the examination of the layers, using the segregation observed in the FM values provided in Table 1 as a basis for analysis. The FM values of the samples exhibited a clear division, with values above and below 2000 MPa. Samples 1, 2, 3, 7, and 10 belonged to the low-FM class, averaging 1866.15 ± 72.16 MPa, while Samples 4, 5, 6, 8, and 9 belonged to the high-FM class, averaging 2435.70 ± 87.94 MPa. Layer photographs were categorized and analyzed based on these low and high-value FM groups, respectively.

In all but one of the low-FM specimens, deformations and deficiencies incurred during layer production were evident. With an average density of 1.06 ± 0.01 g/cm³, these defects, typically observed across multiple layers, were most noticeable in the middle and edge regions of the samples. Examples of these defective layers are illustrated in the Figure 6.

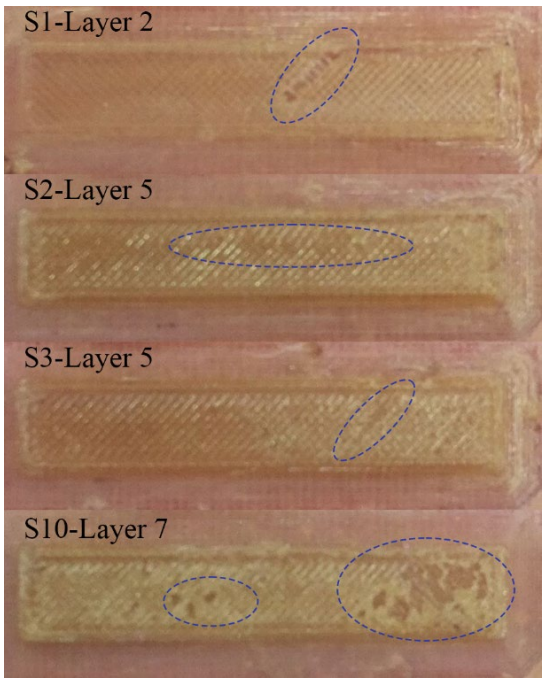

Figure 6. Examples of defective layers in low-FM samples. In the upper left corner of each image, the specific layer number of the sample (S) is indicated.

The most notable sample in this cluster is Sample 7, which exhibits no issues across any of its layers. Remarkably, this nearly flawless specimen has the lowest density and an above-average thickness. This anomaly can be attributed to a relatively high nozzle-to-bed distance and a consistent reduction in filament diameter during printing. Consequently, despite the production process being executed correctly, the low density and weak interlayer adhesion of this sample likely result in a lower FM value.

The samples in the High-FM cluster either exhibit very minor defects or are entirely flawless. Samples 8 and 9 show no issues at all. Sample 4 has only small imperfections in the last layer, and Sample 6 displays a slight mark in the tenth layer. Sample 5 is distinct from the others as it has defects in a few layers; however, these imperfections are located near the edges, well outside the 50 mm span used for FM measurements. Figure 7 illustrates the layer photographs of these High-FM samples, highlighting the minor defects where present.

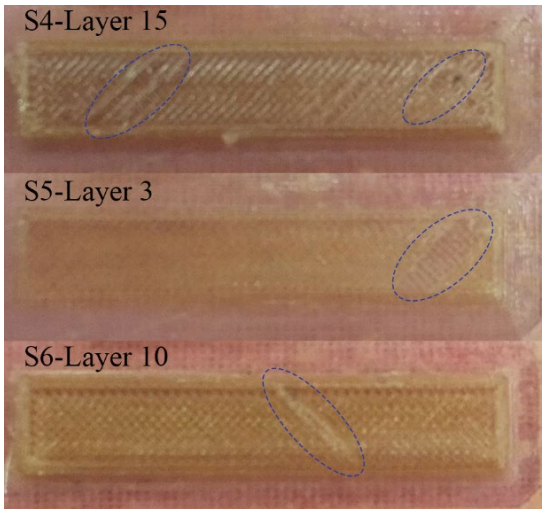

Figure 7. Defective layers in High-FM samples. In the upper left corner of each image, the specific layer number of the sample (S) is indicated.

The case observed in Sample 5 underscores that anisotropy resulting from additive manufacturing can lead to varying mechanical properties depending on the specific use and purpose of the fabricated product. This observation further emphasizes the critical importance of maintaining high production quality. In this context, the next section discussed the impact of production parameters, monitored via sensors, on the final products.

3.5. Sensor Data Analysis

Sensor data was collected for four different physical quantities. Two of these are the nozzle temperature and bed temperature, which were obtained from the log records of Marlin, the 3D printer's control software, and were entered as fixed values. The other two measurements are the chamber temperature and relative humidity, recorded by the BME280 sensor and collected from the log records of the OctoPrint software. Unlike the fixed nozzle and bed temperatures, these values vary and reflect the in-cabinet conditions during printing, particularly in relation to the bed temperature.

For the four monitored quantities, the mean values obtained across all samples were 375.062 ± 0.203 °C for nozzle temperature, 160.004 ± 0.009 °C for bed temperature, 80.544 ± 0.937 °C for chamber temperature, and 3.952 ± 0.106 % for relative humidity.

Sensor data from the production of 3D printed PEI samples can be seen in the Figure 8 as box charts. The graphs in the figure visualize the distributions of nozzle temperature, bed temperature, chamber temperature, and relative humidity data. Each plot displays the median, quartile values (25%-75%), mean values, and outliers identified according to the 1.5 IQR method. The green boxes represent the central tendency and spread of each sample, circle symbols denote the mean values, and the whiskers indicate the range of the data, including outliers.

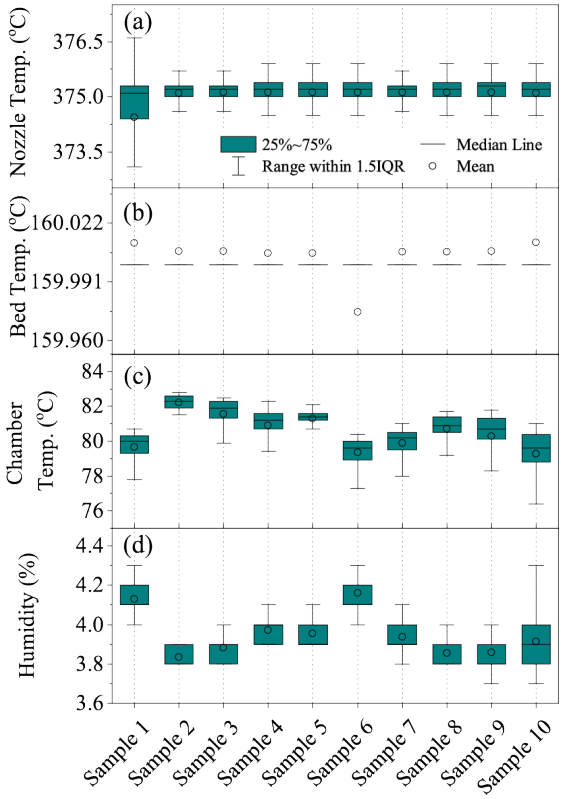

Figure 8. Box charts of sensor data from the production of 3D printed PEI samples: (a) Nozzle temperature, (b) Bed temperature, (c) Chamber temperature and (d) Relative Humidity.

When analyzing the nozzle temperature data, it was observed that the temperature remained stable around the target value of 375 °C. Both

the median and mean values were remarkably close to 375 °C, with the data distribution concentrated within a narrow range. This indicates that the Nozzle temperature was well-maintained. However, some samples contained outliers, identified using the 1.5 IQR method, suggesting occasional temperature fluctuations.

For the bed temperature data, the values were centered around the target temperature of 160°C. The median and mean values were generally close to 160°C, with minor deviations. Outliers in some samples indicated unexpected fluctuations in temperature control.

Analysis of the chamber temperature data revealed a range of 70 – 80 °C across samples. Differences between the median and mean values suggested potential asymmetries in the data distribution. The data spread over a wide range, with outliers indicating that chamber temperature might fluctuate due to environmental factors or equipment condition during the production process.

Relative humidity data showed variation between 3.9% and 4.8% among samples. The median and mean values were remarkably close, with a narrow distribution range, indicating general stability in moisture levels. However, outliers were detected in certain samples according to the 1.5 IQR method, indicating occasional unexpected fluctuations in humidity levels. In conclusion, the analyzed physical quantities were generally stable, but certain samples exhibited unexpected fluctuations and outliers.

3.6. Relationship Between Sensor Data, Physical Properties and Flexural Moduli

For the correlation analysis between sensor data and physical measurements, the distribution and relationships of the data were first assessed to determine the most appropriate correlation methods. A preliminary examination using scatter plots, which were not included here to save space, revealed mostly non-linear relationships and the presence of some outliers. Consequently, Pearson correlation was deemed unsuitable due to its assumption of linearity. Instead, Spearman and Kendall correlations were identified as more appropriate for this analysis.

The results of the Spearman and Kendall correlation analyses are presented in Table 3, which includes both correlation values and p-values for each pair. The Spearman correlation analysis showed significant results for the variable pairs nozzle temperature and width, and nozzle temperature and length, suggesting potential monotonic relationships between these pairs. Both Spearman and Kendall correlations indicated significant results for bed temperature and mass, and bed temperature and density, implying consistent order-based relationships in these pairs. Additionally, the Spearman correlation revealed a significant result for the enclosure temperature and length pair, indicating a potential monotonic relationship.

Table 3. Correlation Analysis Results between Sensor Data and Physical Dimensions with p-values in parentheses.

Coor.	Feature	Nozzle Temp.	Bed Temp.	Cham. Temp.	Hum.
Spearman Correlation	Thickness	-0.204 (0.571)	0.215 (0.551)	0.180 (0.620)	-0.099 (0.785)
	Width	0.498 (0.143)	-0.471 (0.169)	0.298 (0.403)	-0.182 (0.614)
	Length	0.559 (0.093)	-0.550 (0.099)	0.517 (0.126)	-0.116 (0.751)
	Mass	0.539 (0.108)	-0.622 (0.055)	0.103 (0.777)	0.152 (0.676)
	Density	0.552 (0.098)	-0.634 (0.049)	0.309 (0.385)	-0.079 (0.829)
Kendall Correlation	Thickness	-0.167 (0.520)	0.220 (0.405)	0.119 (0.646)	-0.072 (0.783)
	Width	0.405 (0.106)	-0.322 (0.205)	0.180 (0.473)	-0.135 (0.590)
	Length	0.449 (0.072)	-0.414 (0.103)	0.315 (0.209)	-0.135 (0.590)
	Mass	0.333 (0.216)	-0.432 (0.087)	0.067 (0.862)	0.156 (0.601)
	Density	0.422 (0.108)	-0.523 (0.038)	0.156 (0.601)	-0.022 (1.000)

To accurately evaluate the relationship between sensor data and flexural modulus (FM), an appropriate method must be employed. FM, an intrinsic property of the material, was measured individually for each sample, independent of physical dimensions. However, the analyses revealed that FM values were distributed into two distinct clusters, which were strongly correlated with the density of the samples. Defects such as filament diameter fluctuations,

bed and nozzle misalignment, and incomplete layer production were identified as contributing factors. To address this issue, although not a complete solution, the relationship between sensor data and FM was analyzed using normalized FM values, obtained by dividing the FMs by the density values.

For the correlation analysis between the sensor data and FM_{Norm} (normalized flexural moduli), the distribution and relationships of the data were first analyzed using scatter plots, which are not presented here. Preliminary examination showed that the data showed mostly non-linear relationships and some outliers were present. This once again showed that Pearson's correlation may not be suitable due to the linearity assumption, whereas Spearman and Kendall correlations may give more meaningful results.

Table 4 presents Spearman and Kendall correlation coefficients alongside their respective p-values for the relationships between sensor data (nozzle, bed and chamber temperatures, and humidity) and FM_{Norm}. Significant monotonic relationships were identified between the nozzle and bed temperatures and FM_{Norm}. The Spearman correlation for nozzle temperature is 0.685 ($p = 0.029$), and for bed temperature, it is -0.744 ($p = 0.014$), indicating medium strength and significant correlations.

Table 4. Spearman and Kendall Correlation Analysis between sensor data and normalized flexural moduli (FM_{Norm}) with p-values in parentheses.

Sensor	Spearman Correlation	Kendall Correlation
Nozzle Temp.	0.685 (0.029)	0.511 (0.047)
Bed Temp.	-0.744 (0.014)	-0.568 (0.024)
Chamber Temp.	-0.200 (0.580)	-0.111 (0.727)
Humidity	0.285 (0.425)	0.156 (0.601)

Similarly, the Kendall correlation analysis shows significant relationships for nozzle and bed temperatures. The Kendall correlation for nozzle temperature is 0.511 ($p = 0.047$), and for bed temperature, it is -0.568 ($p = 0.024$). These findings confirm that nozzle and bed temperatures are significantly correlated with FM_{Norm} in terms of ranking consistency. No significant correlations were found for chamber temperature and humidity data, as both Spearman and Kendall correlations and p-values indicate no significant relationships with FM_{Norm}.

In addition to correlation analyses, ANOVA was performed to investigate the relationships between the FM_{Norm} and the sensor data. Despite the lack of strong correlations, one-way and several multivariate ANOVA models were examined, the models of which are given below:

1) $FM_{Norm} \sim$ Nozzle
2) $FM_{Norm} \sim$ Bed
3) $FM_{Norm} \sim$ Chamber
4) $FM_{Norm} \sim$ Humidity
5) $FM_{Norm} \sim$ Nozzle + Bed + Chamber + Humidity
6) $FM_{Norm} \sim$ Nozzle × Bed × Chamber × Humidity
7) $FM_{Norm} \sim$ Nozzle × Bed × Chamber
8) $FM_{Norm} \sim$ Nozzle × Bed × Humidity
9) $FM_{Norm} \sim$ Nozzle × Bed
10) $FM_{Norm} \sim$ Nozzle + Bed + Chamber + Humidity + $Nozzle^2$ + Bed^2 + $Chamber^2$ + $Humidity^2$

ANOVA results were obtained for all models except the sixth model, which produced infinite values and could not be analyzed. To save space, only the key findings are presented here, as many results were not statistically significant.

The one-way ANOVA analyses (models 1-4) examined the effects of nozzle, bed and chamber temperatures, and humidity on FM_{Norm} individually. The effect of nozzle temperature on FM_{Norm} ($F=1.887653$, $p=0.206729$) was not statistically significant. Similarly, the effects of bed temperature ($F=3.866159$, $p=0.084834$), chamber temperature ($F=0.124862$, $p=0.732950$), and humidity ($F=0.233881$, $p=0.641621$) were also found to be non-significant.

In the multivariate model (model 5), which included all sensor variables, none of the variables exhibited a significant effect on FM_{Norm}: nozzle temperature ($F=1.044978$, $p=0.346102$), bed temperature ($F=1.714087$, $p=0.238357$), chamber temperature ($F=0.078238$, $p=0.789092$), and humidity ($F=0.147595$, $p=0.720394$).

When analyzing the interaction between nozzle, bed, and chamber temperatures (model 7), the interaction term Nozzle:Bed (F=1.805673, p=0.250190) and other main effects remained non-significant.
However, in the model examining the interaction between nozzle and bed temperatures, and humidity (model 8), a significant interaction was found for the temperature term (F=9.576104, p=0.036414), while the other interaction terms were not significant.

Further analysis of the interaction between nozzle and bed temperatures (model 9) also revealed no significant results for the nozzle temperature interaction term (F=2.418823, p=0.170884).

Finally, the relationship between FM_{Norm} and the variables nozzle, bed and chamber temperatures, and humidity, along with their squared terms (model 10), was analyzed. None of these variables were found to have a statistically significant effect in this model.

In summary, while some individual and interaction terms approached significance, most of the ANOVA results did not indicate statistically significant relationships between FM_{Norm} and the sensor data. This suggests that other factors or more complex interactions may influence FM, or that the variability in the measurements was too high to detect significant effects with the current dataset. The lack of significance in many results underscores the complexity of additive manufacturing processes and the need for further investigation into other potential influencing factors.

The most significant challenge encountered in these analyses is that the average values of the sensors do not accurately represent the production process. In fact, for a sample production that takes an average of 14.6 minutes, sensor data comprising 3,375 values each are more meaningful when analyzed on a layer-by-layer basis. For a layer that takes an average of 52.3 seconds to complete (excluding the first layers, which take an average of 144 seconds, about 2 and a half minutes, due to the inclusion of skirts and 50% speed reduction), each sensor records approximately 200 different values (an average of 554 values for the first layers). Therefore, an accurate representation of the sensor data must be provided on a per-layer basis.
Within the scope of this study, conclusive results based on mathematical models were not obtained from analyzing sensor data on a layer-by-layer basis to uncover their relationships in physical specifications or production quality. However, a novel method was developed that can geometrically represent a layer's production using sensor data and completely independent of time constraints, which could lead to more precise results with more extensive studies in the future.

3.7. Representative Layer Figures by Sensor Data

A method was developed to correlate the sensor data with the extruder positions (X and Y) and to compare the layer photographs taken during printing for each layer. The algorithm, utilizing the numpy and svgwrite libraries, processes the collected data and generates SVG visualizations that illustrate sensor values across different layers. The primary steps of the algorithm are as follows:

1. The algorithm reads the dataset containing X-Y coordinate data along with sensor values such as nozzle temperature, bed temperature, enclosure temperature, and humidity created by the log files.

2. A function maps the sensor values to RGB color values, which are used to visually represent the different sensor readings in the SVG. For instance, nozzle temperature, with minimum and maximum values of 363.3 °C and 379.3 °C respectively, 379.3 °C is defined as full red (RGB: 255, 0, 0) and 363.3 °C as full black (RGB: 0, 0, 0). For intermediate values, the corresponding red value is determined by linear interpolation between 0 and 255 (e.g., 370°C → RGB: 107, 0, 0).

3. For each layer in the dataset, an SVG file is created. The X and Y coordinates are used to draw lines representing the movements of the 3D printer nozzle, with the line colors indicating the sensor values at those points.

4. The code iterates through all layers, generating individual SVG files for each layer and sensor type. These individual SVGs are then combined into a comprehensive SVG file,

providing a visual representation for a single sample.

An example of the visualization of data collected from a single sensor during the production of a layer is shown in Figure 9. For Sample 1, this visualization clarifies the significant deviation in nozzle temperature observed in Figure 8a. The deviation was a momentary issue during the printing of the first layer, causing the temperature to drop to 363.3 °C and rise to a maximum of 376.3 °C. In fact, this fluctuation occurred only in specific parts of the layer and did not impact the entire layer.

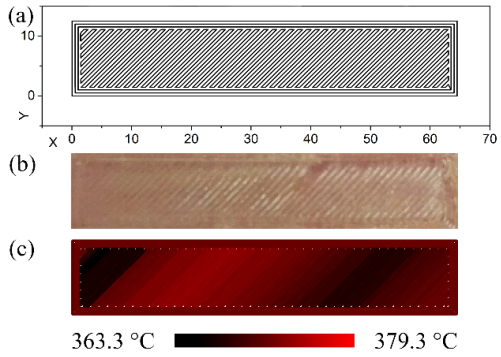

Figure 9. (a) Extruder paths generated from the X-Y coordinates of the first layer without skirt lines, with (b) photograph belongs to the relevant layer and (c) nozzle temperature values along these paths during the production of Sample 1.

The optimal approach for further research involves examining the representative layer figures produced using sensor data alongside the layer photographs. **Figure 10** presents the layer photographs and corresponding sensor data layers for Sample 6, which exhibited the lower flexural modulus (Low-FM) value.

Figure 10 clearly demonstrates that the nozzle temperature, a critical parameter, deviated from the target value during the production of the first and fifth layers. Correspondingly, the layer photographs exhibit printing defects within this range. It appears that the initial defect originates from a gap in the first layer, subsequently affecting the layers above it. This imperfection may be related to the temperature variation, although conclusive evidence is lacking. Additionally, faded surfaces on the left side of the first five-layer photographs can exist because of the temperature drop in the first layer. This temperature variation could have resulted in weaker adhesion to the bed, causing the observed color difference. Alternatively, the bed may not have been perfectly parallel to the nozzle. In both scenarios, thickness variation across the sample is evident, as shown by the standard deviation plots in Figure 4a.

On the other hand, instantaneous fluctuations in humidity are particularly significant for PEI, a thermoplastic highly sensitive to moisture. Notably, a marked decrease in humidity is observed in the fifth layer. This reduction may contribute to the production of relatively higher-quality layers following this point.

Although these interpretations can be made through straightforward observation, the high resolution of the images and the narrow oscillation range of the fixed parameters make these conclusions highly speculative. To establish such relationships with greater precision, a larger number of samples is required. Comprehensive studies with parameters taking multiple values, similar to classical optimization approaches, are essential. By employing advanced data analysis methods such as machine learning and neural networks, these relationships can be more robustly determined.

Finally, to facilitate a comparison between specimens in the Low-FM and High-FM clusters, Figure 11 presents the layer photographs of Sample 8 alongside their corresponding representative layers.

4. CONCLUSION

In this study, a comprehensive critique of the 3D printing process for PEI filament produced in a domestically developed extrusion park using a custom-made 3D printer were conducted. The investigation focused on the diverse outcomes produced by fixed printing parameters under complex influences, without eliminating or selecting specific samples.

The results clearly demonstrated the significant impact of production parameters on the final product quality. In addition to examining physical attributes such as dimensions and density, the study also evaluated the mechanical properties of each specimen through flexural modulus tests, as determined by the chosen specimen geometry. The findings revealed the formation of two distinct clusters (Low- and High-FM). The Low-FM cluster exhibited a 10% reduction in density and a 25% reduction

in flexural modulus compared to the High-FM cluster. These results underscore the necessity for precise control of production parameters, considering the complex and anisotropic nature of additive manufacturing. Correlation analyses between sensor data collected during production and mechanical properties highlighted the critical role of nozzle and bed temperatures in determining product quality. However, none of the variance analyses (ANOVA) models yielded significant results.

The main findings of this study highlight several critical considerations that differentiate this research from previous works in the field. Unlike many studies that focus on parameter optimization by eliminating outliers or selecting specific conditions, this study uniquely explores the variability in outcomes when parameters are kept constant yet subjected to complex and uncontrolled influences. This approach provides a more realistic insight into the challenges of maintaining consistency in additive manufacturing. The detailed analysis of each layer, including photographing and examining potential defects, further distinguishes this study by providing practical methods for improving quality control. Moreover, while some studies have not fully explored the subtle impacts of the nozzle and bed temperature adjustments and fluctuations, this research highlights their role in determining product quality, providing new insights into the importance of these parameters. In addition to temperature control, precise alignment of the nozzle and bed, along with proper surface preparation, especially when using adhesives, has also been identified as essential for achieving optimal production outcomes.

The findings from this study will form the basis for more extensive future research. Further exploration into real-time monitoring with more precise sensors and control of production parameters promises to enhance process efficiency. The use of machine learning and advanced data analysis techniques, supported by the representative layer algorithm, has the potential to reveal complex relationships within manufacturing processes. These innovative approaches will be instrumental in enhancing the consistency of additive manufacturing processes. By demonstrating that varying outcomes can arise in manufacturing processes, even with fixed parameters, this study opens up new avenues for quality control and optimization in additive manufacturing technologies. Future research will build on these findings to enable more effective use of high-performance thermoplastics in industrial applications.

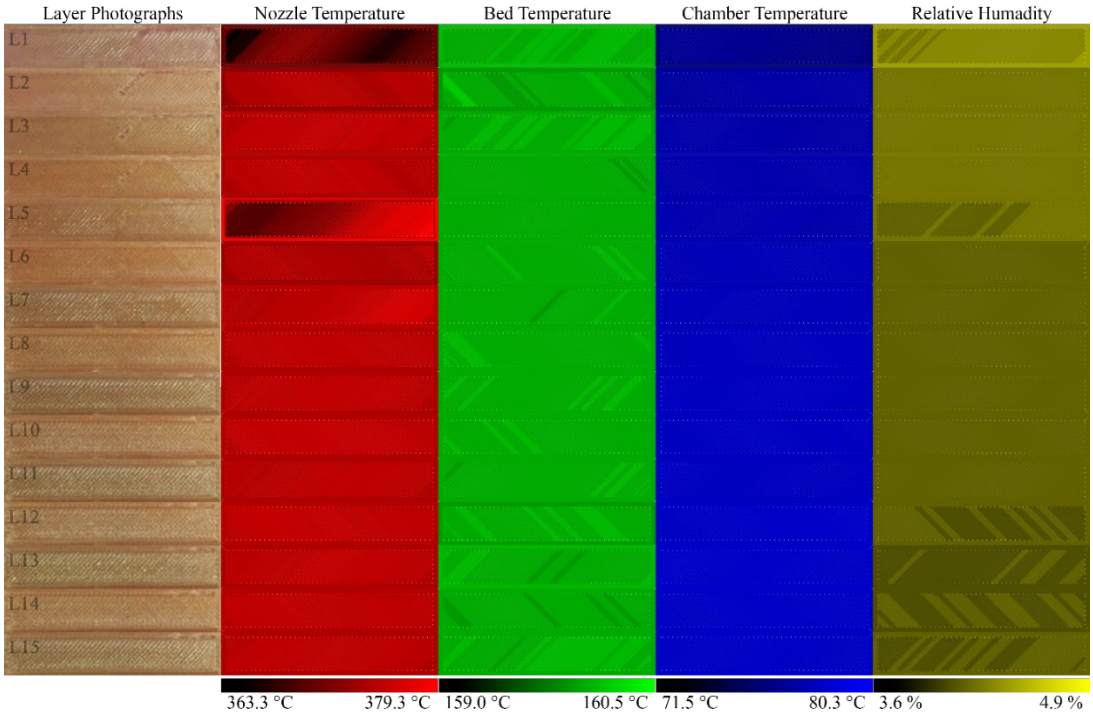

Figure 10. Layer photographs and corresponding sensor data-generated representative layers for Sample 1. The color scale for each sensor is provided below the respective representative layers.

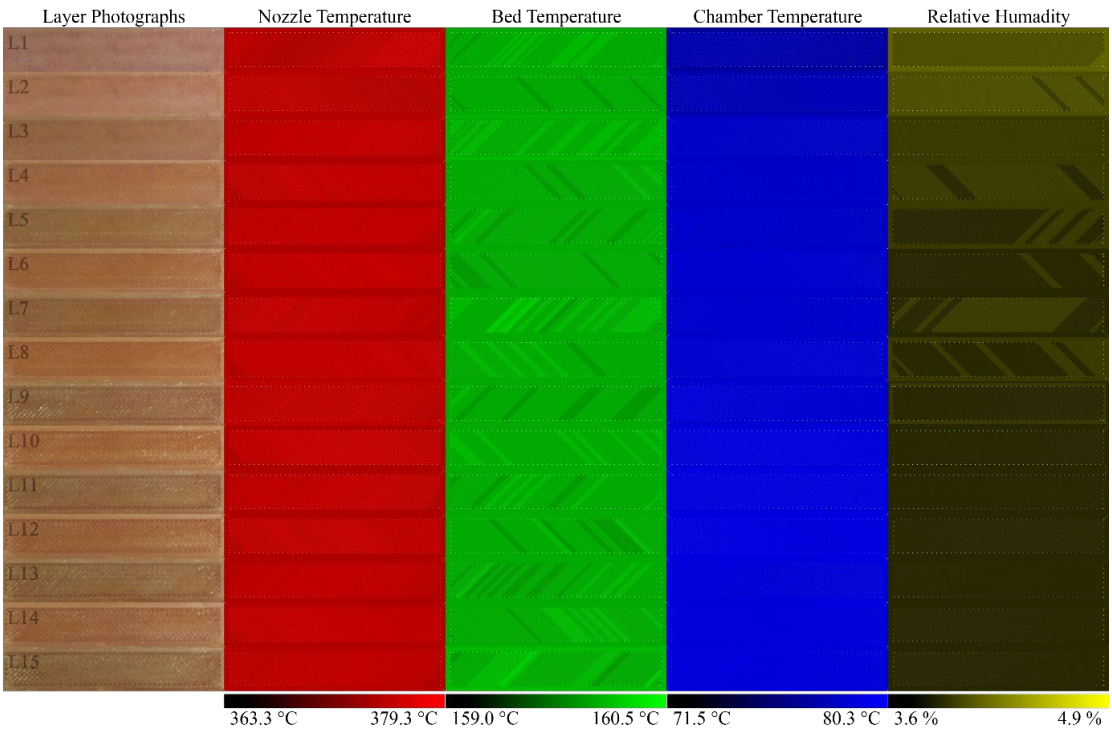

Figure 11. Layer photographs and corresponding sensor data-generated representative layers for Sample 8. The color scale for each sensor is provided below the respective representative layers.

ACKNOWLEDGES

The author would like to thank Uğur Emanetoğlu for his help with 3D printing, Merve Karabal for her help with DMA tests, and Dr. Emre Koyuncu for a thought-provoking discussion on the algorithm of representative layer figures. Special thanks are extended to Dr. Hülya Cebeci for providing access to laboratory facilities and other resources. The study was supported by the ITU BAP Division with project number MAB-2019-42010.

REFERENCES

1. Gao, W., Zhang, Y., Ramanujan, D., Ramani, K., Chen, Y., Williams, C. B., Zavattieri, P. D., "The status, challenges, and future of additive manufacturing in engineering", Computer-Aided Design, Vol. 69, Issue 1, Pages 65-89, 2015.

2. Baumers, M., Dickens, P., Tuck, C., Hague, R., "The cost of additive manufacturing: machine productivity, economies of scale and technology-push", Technological Forecasting and Social Change, Vol. 102, Issue 1, Pages 193-201, 2016.

3. Ford, S., Despeisse, M., "Additive manufacturing and sustainability: an exploratory study of the advantages and challenges", Journal of Cleaner Production, Vol. 137, Issue 1, Pages 1573-1587, 2016.

4. Vakharia, V. S., Leonard, H., Singh, M., Halbig, M. C., "Multi-Material Additive Manufacturing of High Temperature Polyetherimide (PEI)–Based Polymer Systems for Lightweight Aerospace Applications", Polymers, Vol. 15, Issue 3, Pages 561, 2023.

5. Kaynan, O., Yıldız, A., Bozkurt, Y.E., Yenigun, E.O., Cebeci, H., "Electrically conductive high-performance thermoplastic filaments for fused filament fabrication", Composite Structures, Vol. 237, Issue 1, Pages 111930, 2020.

6. Bozkurt, Y.E., Emanetoğlu, U., Yıldız, A., Türkarslan, Ö., Şaşal, F.N., Cebeci, H., "3D printable CNTs and BN hybridized PEEK composites for thermal management applications", Journal of Materials Science, Vol. 58, Issue 38, Pages 15086-15099, 2023.

7. Kim, H., Lin, Y., Tseng, T.-L. B., "A review on quality control in additive manufacturing", Rapid Prototyping Journal, Vol. 24, Issue 3, Pages 645-669, 2018.

8. Strano, M., Farioli, D., Giberti, H., "Extrusion Additive Manufacturing of PEI Pellets", Journal of Manufacturing and Materials Processing, Vol. 6, Issue 6, Pages 157, 2022.

9. Turner, B.N., Strong, R., Gold, S.A., "A review of melt extrusion additive manufacturing processes: I.

Process design and modeling", Rapid Prototyping Journal, Vol. 20, Issue 3, Pages 192-204, 2014.

10. Turner, B.N., Gold, S.A., "A review of melt extrusion additive manufacturing processes: II. Materials, dimensional accuracy, and surface roughness", Rapid Prototyping Journal, Vol. 21, Issue 3, Pages 250-261, 2015.

11. Go, J., Schiffres, S.N., Stevens, A.G., Hart, A.J., "Rate limits of additive manufacturing by fused filament fabrication and guidelines for high-throughput system design", Additive Manufacturing, Vol. 16, Issue 1, Pages 1-11, 2017.

12. Sun, X., Mazur, M., Cheng, C.-T., "A review of void reduction strategies in material extrusion-based additive manufacturing", Additive Manufacturing, Vol. 67, Issue 1, Pages 103463, 2023.

13. Kuruoğlu, Y., Akgün, M., Demir, H., "FDM Yöntemiyle Üretilen ABS, PLA ve PETG Numunelerin Yüzey Pürüzlülüğü ve Çekme Dayanımının Modellenmesi ve Optimizasyonu" [Modelling and Optimization of Surface Roughness and Tensile Strength of ABS, PLA and PETG Samples Produced by FDM Method] [article in Turkish], International Journal of 3D Printing Technologies and Digital Industry, Vol. 6, Issue 3, Pages 358-369, 2022.

14. Albaşkara, M., Türkyılmaz, S., "Optimization of Accuracy and Surface Roughness of 3D SLA Printed Materials with Response Surface Method", International Journal of 3D Printing Technologies and Digital Industry, Vol. 7, Issue 3, Pages 403-414, 2023.

15. Jiang, S.; Liao, G.; Xu, D.; Liu, F.; Li, W.; Cheng, Y.; Li, Z.; Xu, G., "Mechanical properties analysis of polyetherimide parts fabricated by fused deposition modeling", High Performance Polymer, Vol. 31, Issue 1, Pages 97–106, 2019.

16. Ding, S.; Zou, B.; Wang, P.; Ding, H., "Effects of nozzle temperature and building orientation on mechanical properties and microstructure of PEEK and PEI printed by 3D-FDM", Polymer Testing, Vol. 78, Issue 1, Pages 105948, 2019.

17. Forés-Garriga, A.; Pérez, M.A.; Gómez-Gras, G.; Pozo, G.R., "Role of infill parameters on the mechanical performance and weight reduction of PEI Ultem processed by FFF", Materials and Design, Vol. 193, Issue 1, Pages 108810, 2020.

18. Bozkurt, Y.E., Kincal, C., Yüksel, R., Yildiz, A., Solak, N., Cebeci, H., "3D Printable BN/PEEK/PEI Polymer Blend Composites for Thermal Management Applications", AIAA SCITECH 2024 Forum, Pages 0368, 2024.

19. El Magri, A.; Vanaei, S.; Vaudreuil, S., "An overview on the influence of process parameters through the characteristic of 3D-printed PEEK and PEI parts", High Performance Polymers, Vol. 33, Issue 1, Pages 862–880, 2021.

20. El Magri, A.; Mabrouk, K.E.; Vaudreuil, S., "Preparation and characterization of poly (ether ether ketone)/poly (ether imide) [PEEK/PEI] blends for fused filament fabrication", Journal of Materials Science, Vol. 56, Issue 1, Pages 14348–14367, 2021.

21. Vanaei, H.R., Shirinbayan, M., Deligant, M., Khelladi, S., Tcharkhtchi, A., "In-Process Monitoring of Temperature Evolution during Fused Filament Fabrication: A Journey from Numerical to Experimental Approaches", Thermo, Vol. 1, Issue 3, Pages 332-360, 2021.

22. Sgrulletti, M., Bragaglia, M., Giarnetti, S., et al., "Understanding the Impact of Fused Filament Fabrication Conditions on the Microstructure and Tensile Properties of Polyamide 6 by Thermal and Optical Live Monitoring", Materials Today Communications, Vol. 28, Issue 1, Pages 102679, 2021.

23. Alatefi, M., Al-Ahmari, A.M., AlFaify, A.Y., Saleh, M., "A Framework for Multivariate Statistical Quality Monitoring of Additive Manufacturing: Fused Filament Fabrication Process", Processes, Vol. 11, Issue 4, Pages 1216, 2023.

24. Özsoy, K., Aksoy, B., "Real-Time Data Analysis with Artificial Intelligence in Parts Manufactured by FDM Printer Using Image Processing Method", Journal of Testing and Evaluation, Vol. 50, Issue 1, Pages 629-645, 2022.

25. Yıldız, A., Emanetoğlu, U., Yenigun, E.O., Cebeci, H., "Towards optimized carbon nanotubes (CNTs) reinforced polyetherimide (PEI) 3D printed structures: A comparative study on testing standards", Composite Structures, Vol. 296, Issue 1, Pages 115853, 2022.